Published in final edited form as:
J Am Chem Soc. 2010 June 9; 132(22): 7638–7644. doi:10.1021/ja909923w.

Redox Potential and C-H Bond Cleaving Properties of a Nonheme Fe^{IV}=O Complex in Aqueous Solution

Dong Wang[#,‡], **Mo Zhang**[#,‡], **Philippe Bühlmann**[#,*], and **Lawrence Que Jr.**[#,‡,*]

[#]Department of Chemistry, University of Minnesota, Minneapolis, MN, 55455 USA

[‡]Center for Metals in Biocatalysis, University of Minnesota, Minneapolis, MN, 55455 USA

Abstract

High-valent iron-oxo intermediates have been identified as the key oxidants in the catalytic cycles of many nonheme enzymes. Among the large number of synthetic Fe^{IV}=O complexes characterized to date, $[Fe^{IV}(O)(N4Py)]^{2+}$ (**1**) exhibits the unique combination of thermodynamic stability, allowing its structural characterization by X-ray crystallography, and oxidative reactivity sufficient to cleave C-H bonds as strong as those in cyclohexane (D_{C-H} = 99.3 kcal mol^{-1}). However, its redox properties are not yet well understood. In this work, the effect of protons on the redox properties of **1** has been investigated electrochemically in nonaqueous and aqueous solutions. While the cyclic voltammetry of **1** in CH_3CN is complicated by coupling of several chemical and redox processes, the $Fe^{IV/III}$ couple is reversible in aqueous solution with $E_{1/2}$ = +0.41 V vs. SCE at pH 4 and involves the transfer of one electron and one proton to give the Fe^{III}-OH species. This is in fact the first example of reversible electrochemistry to be observed for this family of nonheme oxoiron(IV) complexes. C-H bond oxidations by **1** have been studied in H_2O and found to have reactions rates that depend on the C-H bond strength but not on the solvent. Furthermore, our electrochemical results have allowed a D_{O-H} value of 78(2) kcal mol^{-1} to be calculated for the Fe^{III}-OH unit derived from **1**. Interestingly, although this D_{O-H} value is 6-11 kcal mol^{-1} lower than those corresponding to oxidants such as $[Fe^{IV}(O)(TMP)]$ (TMP = tetramesitylporphinate), $[Ru^{IV}(O)(bpy)_2(py)]^{2+}$ (bpy = bipyridine, py = pyridine) and the *tert*-butylperoxyl radical, the oxidation of dihydroanthracene by **1** occurs at a rate comparable to those for these other oxidants. This comparison suggests that the nonheme N4Py ligand environment confers a kinetic advantage over the others that enhances the C-H bond cleavage ability of **1**.

1. Introduction

Nonheme high-valent iron-oxo intermediates have been identified as the key oxidants that carry out substrate oxidations in the catalytic cycles of many nonheme enzymes.[1-4] In the past decade, a large number of synthetic Fe^{IV}=O complexes supported by polydentate ligands has been reported, shedding light on the electronic structures and properties of the novel Fe^{IV}=O unit.[5-7] To date the structures of three synthetic Fe^{IV}=O complexes have been obtained by X-ray crystallography.[8-10] Among these three, only $[Fe^{IV}O(N4Py)]^{2+}$ (**1**) (N4Py = *N*,*N*-bis(2-pyridylmethyl)-bis(2-pyridyl)methylamine) (see Figure 1) has shown the ability to oxidize C-H bonds as strong as those in cyclohexane (D_{C-H} = 99.3 kcal mol^{-1}).[11,12]

larryque@umn.edu, buhlmann@umn.edu.

Supporting Information Available. Figure S1-S3; Table S1, S2 and digital simulation parameters. This material is available free of charge via the internet at http://pubs.acs.org.

The oxidizing power of **1** has stimulated efforts to establish its redox potential in order to rationalize its high C-H bond cleaving reactivity.[13-15] However, the redox behavior of **1** is complicated and not straightforward to interpret. For example, in initial cyclic voltammetric (CV) experiments in dry CH_3CN, **1** exhibited only a reductive wave at $E_{p,c}$ = -0.44 V vs. $Fc^{+/0}$, with no corresponding oxidative peak.[13,14] Interestingly the observed $E_{p,c}$ value was substantially more negative than the $E_{1/2}$ value associated with the reversible $Fe^{III/II}$ couple of $[Fe^{II}(N4Py)(CH_3CN)]^{2+}$ (**2**, +0.61 V vs. $Fc^{+/0}$) measured in CH_3CN,[16,17] which seemed contradictory to the high oxidizing ability of **1** towards hydrocarbons. Lee *et al.* subsequently assigned an $E_{1/2}$ value of +0.51 V vs. SCE (or +0.11 V vs. $Fc^{+/0}$) for **1** by averaging the $E_{p,c}$ of the reductive wave at -0.44 V vs. $Fc^{+/0}$ and the $E_{p,a}$ value of an oxidative peak that was observed at a one-volt higher potential but exhibited a much smaller current than the reductive wave.[15] Using a spectropotentiometric method, Collins *et al.* determined the $E_{1/2}$ for **1** in CH_3CN in the presence of 0.1 M H_2O and found a value of +0.90 V vs. $Fc^{+/0}$, suggesting a significant effect of water.[14] As this experiment could only be carried out for the oxidation of the Fe^{III}-OH species to **1**, what was actually measured was the oxidation potential of the Fe^{III}-OH species, rather than the reduction potential of the Fe^{IV}=O unit. The different values associated with the $Fe^{IV/III}$ redox couple of **1** thus far reveal the complexity of the 1-e^- reduction process of the Fe^{IV}=O unit in CH_3CN.

That the presence of a proton donor should have an effect on the $Fe^{IV/III}$ redox couple is not surprising. It is well known from classic electrochemical studies of benzoquinone/hydroquinone[18] and dioxygen species (O_2, HO_2•, H_2O_2)[19] in aqueous solutions that the availability of protons dramatically affects the potential at which electron transfer occurs in a process where electron transfer (ET) is associated with proton transfer (PT). A Pourbaix plot that correlates the measured potential $E_{1/2}$ and pH can be constructed to determine the stoichiometry of the electron and proton transferred in the redox process. The standard redox potentials (E°) and acid dissociation constants (pK_a) of species in different protonated forms can be determined from the crossing points of the linear sections with different slopes. For metal-oxo complexes, similar precedents can be found in electrochemical studies of Ru^{IV}=O complexes supported by polypyridine-based ligands, where no $Ru^{IV/III}$ couple could be detected in CH_3CN or CH_2Cl_2.[20] However, by switching from nonaqueous to aqueous solution, the CV behavior became straightforward to interpret, and a reversible $Ru^{IV/III}$ couple was observed in the pH range of 2–10 with a redox potential dependent on the pH of the solution.[20-24] This work on Ru^{IV}=O complexes suggested the possibility that a similar electrochemical behavior could also be observed for Fe^{IV}=O complexes in aqueous solution. In this paper, we report detailed electrochemical studies of **1** and examine the effect of protons on its redox properties in nonaqueous and aqueous solutions. Our results reveal that in aqueous solution the 1-e^- reduction of the Fe^{IV}=O unit is associated with the transfer of one proton to form the Fe^{III}-OH species. The rates of C-H bond cleaving reactions by **1** have also been measured in aqueous solution and show that the oxidizing ability of **1** is independent of solvent. Furthermore, comparisons of the C-H bond cleaving rates of **1** and other metal-oxo complexes suggest that the nonheme Fe^{IV}=O complex **1** may have a kinetic advantage in the rate-determining hydrogen atom abstraction step.

2. Experimental Section

General Materials and Procedures

All chemicals are of the highest commercially available purity and were used as received, unless noted otherwise. CH_3CN and butyronitrile were distilled from CaH_2 under Ar before use. Ligand N4Py and complex **1** were synthesized via reported procedures.[11,25] Complex **1** were precipitated as the perchlorate salt and redissolved in CH_3CN or H_2O before each use. CAUTION: The perchlorate salt is potentially explosive and should be handled with care!

Physical Methods

UV-vis spectra were recorded with a Hewlett-Packard 8453A diode array spectrometer equipped with a Unisoku Scientific Instruments cryostat (Osaka, Japan) for temperature control. Cyclic voltammetry (CV) was performed on a CS-1200 Computer-Controlled Potentiostat Electroanalytical System from Cypress Systems, Inc. (Lawrence, Kansas) in dry CH_3CN (0.10 M potassium hexaflurophosphate (KPF_6) as supporting electrolyte) and H_2O (0.10 M sodium perchlorate ($NaClO_4$) as supporting electrolyte) in a standard three electrode cell. CH_3COOH/CH_3COONa buffer (initial CH_3COONa concentration was 0.1 M, and CH_3COOH was added to lower the pH) was used to control the pH value between 3 and 6, while CF_3COOH was used to adjust the pH to values lower than 3. An Orion 8115BN pH electrode from Thermo Fisher Scientific (Waltham, MA) was used to measure the pH. CV simulations and fits were obtained using DigiElch, version 4.M (Elchsoft, Germany).

Kinetic Studies

Reactivity studies in H_2O were carried out in air unless otherwise stated. For a typical experiment, an excess amount of substrate was injected into a 1 cm pathlength UV cuvette containing a freshly prepared solution of **1**. The reaction was monitored by UV-vis spectroscopy following the absorption change at 695 nm in CH_3CN and 680 nm in H_2O. The time traces were fitted to a pseudo-first-order mode to obtain k_{obs} values, and the k_2 value for each substrate was obtained from the slope of the linear fits of the plot of k_{obs} vs. the concentration of the substrate.

3. Results and Discussion

It has been shown that the presence of protons affects the redox behavior of the nonheme Fe^{IV}=O unit.[14,26] This effect is also illustrated by Figure 1, which shows cyclic voltammograms of **1** in CH_3CN in the presence of CF_3COOH as proton donor. With no added CF_3COOH, a cathodic scan elicited a reductive wave with $E_{p,c}$ = -0.13 V vs. SCE (or -0.53 V vs. $Fc^{+/0}$) (Figure 1, top trace), consistent with previously reported values;[13,14] no oxidative wave was observed on the reverse scan. The reductive peak exhibited a sizeable anodic/positive shift with increasing amounts of added CF_3COOH, reaching a value of +0.78 V at 5 M acid (Figure 1، Table S1). Even in the presence of 5 M CF_3COOH, **1** retained its characteristic visible spectrum with λ_{max} at 695 nm with an unchanged extinction coefficient and had a lifetime of several hours at 25 °C, showing that protonation of the Fe^{IV}=O unit did not occur to any significant extent. Upon scan reversal, an oxidative wave was observed when acid was present, with an invariant peak potential $E_{p,a}$ = +1.03 V; this feature did not appear unless the reductive wave at more negative potential was first observed in the cathodic scan. The oxidative wave first appeared with 0.003 M added CF_3COOH, reached a maximum peak current at 0.03–2 M CF_3COOH, but shrank at 5 M CF_3COOH (Figure 1). This $E_{p,a}$ feature can be assigned to the 1-e^- oxidation of the Fe^{II} complex **2**, as shown in previous studies,[14,16,17] an assignment supported by control CV experiments on **2** in the presence of different amounts of CF_3COOH (Figure S1). This observation implies that the cathodic scan produces the Fe^{II} complex **2** from the Fe^{IV} species **1** via an overall 2-e^- reduction process; **2** was then oxidized by 1-e^- to its Fe^{III} form in the reverse anodic scan. This 2:1 stoichiometry of the transferred electrons represented by the reductive and oxidative peaks was confirmed by the integration of both peaks of the CV traces observed in the presence of 0.03–2 M added acid, which revealed that the peak area for the reductive wave was twice as large as that for the oxidative wave.

A mechanism to rationalize the overall redox behavior is proposed in Scheme 1, where **1** is first reduced by one electron and accepts a proton from the added acid to form the corresponding Fe^{III}–OH species. The latter then undergoes an overall process that involves a second 1-e^-reduction, a second protonation and exchange of the aqua ligand by CH_3CN to afford the

product complex **2**. This hypothesis was supported by the good fits of the CV traces measured with 0.03– 2 M added acid (Figure 2). All these fits were performed by applying the reaction mechanism outlined in Scheme 1 and using one single set of kinetic parameters for all acid concentrations in the 0.03–2 M range (see Supporting Information for simulation details), thereby showing that Scheme 1 is consistent with the observed CVs. There are several important observations from the simulations. First, the anodic peak at +1.03 V due to the oxidation of **2** can only be observed when the three coupled chemical equilibria leading to the formation of **2**, i.e., the two proton transfers and the ligand exchange, are sufficiently thermodynamically favorable and kinetically established fast enough to reach an appreciable concentration of **2** within the timeframe of a single CV scan. Secondly, as the first protonation step facilitates the second 1-e^- reduction, the two reduction steps lead to two overlapping CV peaks that are observed as one feature in the cathodic scan. Thirdly, because both e^- transfers are associated with a protonation equilibrium, the peak position of the experimentally observed cathodic peak has a distinct dependence on the proton activity. However, as is well known from analogous and well studied cases such as benzoquinone,[18] it is not possible to determine pK_a and E° values independently when only data of coupled H^+ and e^- transfers are available. This is also confirmed by CV simulations based on Scheme 1, which show that changes in the numerical value of E° for the reduction of Fe^{IV}=O and in the pK_a value of Fe^{III}–OH shift the peak maximum and affect the shape of the cathodic peak in the same way.

Outside the 0.03–2 M acid concentration window, at least one process either competes with the formation of **2** or results in its decomposition, as evident from the smaller oxidation peak in the reverse scan (see Figure 1). The key result is that reduction of **1** is facilitated by an increase in acid concentration. In fact, a plot of the $E_{p,c}$ values vs. -log [CF_3COOH] is linear with the slope of -180 mV per log unit (Figure S2). Because all the CVs shown in Figure 2 can be fitted with the same set of kinetic parameters but with a variable apparent $E_{1/2}$, the shift in $E_{p,c}$ does not have a kinetic origin but rather is the result of a chemical equilibrium coupled to the e^- transfer. The slope of -180 mV per log unit is not currently understood but may be caused by the formation of aggregates involving the acid and its conjugate base in this nonprotic solvent, resulting in a nontrivial dependence of the free proton and anion activities on the total CF_3COOH concentration. Further studies will be required to explain these CVs quantitatively.

In contrast, CV experiments on **1** carried out in pH-buffered aqueous solution are more easily interpreted and provide valuable insight. Complex **1** is soluble in H_2O and quite stable, with a half-life ($t_{1/2}$) ≈ 10 h at 25 °C and pH 7 (vs. 60 h in CH_3CN11). Remarkably, experiments performed in the pH range 1.5–4 revealed a reversible 1-e^- redox couple for **1** (ΔE = 0.06 V, $I_{p,c}/I_{p,a} \approx 1$) (Figure 3). This is the first instance where a reversible wave has been observed for the $Fe^{IV/III}$ couple of a member of the growing family of synthetic nonheme Fe^{IV}=O complexes. Within the range of scan rates from 0.05 to 0.5 V s^{-1}, this process exhibits the proportionality of $I_{p,c}$ and $I_{p,a}$ to the square root of the scan rate (Figure 4, inset), as expected for a freely diffusing species; furthermore, $E_{1/2}$ is independent of the scan rate (Figure 4). These experiments show that the electron transfer associated with the $Fe^{IV/III}$ couple is fully reversible. At pH 4, $E_{1/2}$ was determined to be +0.41 V vs. SCE, a value that was found to shift anodically as the pH was decreased from 4 to 1.5 (Figure 3). As shown in Figure 5, the Pourbaix plot corresponding to this set of data (Table S1) is linear with a slope of -55 mV per pH unit, clearly demonstrating that the 1-e^- reduction of **1** is associated with the transfer of one proton. This interpretation is further supported by the good fits of the CV traces using the reaction mechanism shown in Scheme 1 and a single set of parameters (Figure 3) (see Supporting Information for simulation details). Thus the reduction of **1** under these conditions is best described as a process that converts the Fe^{IV}=O unit to the Fe^{III}–OH species involving the transfer of one electron and one proton.[27]

Below pH 1.5, the oxidative wave on the reverse scan disappeared (Figure S3), likely due to the facile protonation of the Fe^{III}–OH species on the CV time scale. At pH 4–6, the $Fe^{IV/III}$ redox couple exhibited a peak separation of 0.06-0.08 V (Figure S3), close to the value expected for a fully reversible 1-e^- transfer, but the anodic peak current was not as large as the cathodic peak current ($I_{p,c}/I_{p,a} > 1$), suggesting the decay of the Fe^{III}-OH species via an as yet unidentified pathway. Nevertheless, in view of observed peak separations associated with a quasi-reversible couple, the $E_{1/2}$ values obtained at pH 4–6 still fall nicely on the line in the Pourbaix plot (Figure 5). Within this limited pH range, the plot did not exhibit a change in slope that could be used to determine a pK_a, unlike what has been documented in studies of Ru^{IV}=O complexes.[20-24] Therefore, the true E° value of the Fe^{IV}=O/Fe^{III}–O^- couple and the pK_a of the Fe^{III}–OH species cannot be determined independently. (Consequently, the set of numerical values for E_1' and pK_a used for the fits shown in Figure 3 is just one of many sets of $E_{1/2}$ and pH values consistent with the experimental observations.)

With a reversible $Fe^{IV/III}$ couple established for **1** in aqueous solution, its redox potential can now be compared with the handful of values obtained for related iron porphyrin and ruthenium complexes in aqueous solution. A reversible $Fe^{IV/III}$ couple was observed for [Fe^{IV}(O)(TSMP)] (TSMP = tetra(3-sulfonatomesitylporphinate)) at pH 8 with an $E_{1/2}$ value of 0.7 V vs. SCE.[28,29] Between pH 8 and 10, its $Fe^{IV/III}$ potential exhibits the Nernstian pH dependence associated with the transfer of one electron and one proton similar to that found for **1**. Similarly, a reversible $Ru^{IV/III}$ couple was observed for $[Ru^{IV}(O)(bpy)_2(py)]^{2+}$ (bpy = bipyridine, py = pyridine) at pH 7 with an $E_{1/2}$ value of 0.53 V vs. SCE,[21] which falls in the range (0.5–0.8 V vs. SCE) documented for other Ru^{IV}=O complexes supported by polypyridine-based ligands at pH 7.[23,24] Extrapolation of the Pourbaix plot in Figure 5 to pH 7 and 8 gives respective $E_{1/2}$ values of 0.24 and 0.18 V vs. SCE for **1**. These potentials are significantly lower than found for [Fe^{IV}(O)(TSMP)] and $[Ru^{IV}(O)(bpy)_2(py)]^{2+}$, suggesting that **1** has a lower thermodynamic driving force for oxidation than the related iron porphyrin and ruthenium complexes. The availability of these values allows us to assess these complexes with respect to their ability to cleave C-H bonds.

The reactivity of **1** towards C-H bonds in CH_3CN has been well documented, showing that it can even cleave the strong C-H bonds of cyclohexane ($D_{C\text{-}H}$ = 99.3 kcal mol^{-1}).[11,12] Furthermore, there is a linear correlation between the logarithm of the second order rate constants for hydrocarbon oxidation normalized on a per hydrogen basis (log k_2') and the strength of the C-H bond being cleaved ($D_{C\text{-}H}$) (Figure 6). Because of the reversible electrochemical behavior of **1** in H_2O, we have investigated the C-H bond cleavage reactivity of **1** in H_2O for comparison with data obtained in CH_3CN. We chose three water-soluble substrates with a range of $D_{C\alpha\text{-}H}$ values, namely allyl alcohol ($D_{C\alpha\text{-}H}$ = 82 kcal mol^{-1}), THF ($D_{C\alpha\text{-}H}$ = 92 kcal mol^{-1}) and methanol ($D_{C\alpha\text{-}H}$ = 96 kcal mol^{-1}) for the kinetic measurements. At room temperature and under aerobic conditions, **1** reacted with an excess amount of substrate in a pseudo-first order manner, as expected. Second order rate constants (k_2) were obtained from the slope of the linear correlation between the pseudo-first order rate constant (k_{obs}) and the substrate concentration, as shown in Table S2. Remarkably, the log k_2' values obtained in H_2O fell nicely onto the line previously drawn for the correlation between log k_2' in CH_3CN and $D_{C\text{-}H}$ (Figure 6). In addition, the oxidation rate of allyl alcohol by **1** was found to be independent of the pH of the reaction medium (Table S2). These results clearly demonstrate that the reaction rates of **1** with C-H bonds of varying strength are independent of the solvent.

With the above electrochemical information in hand, the $D_{O\text{-}H}$ for $[(N4Py)Fe^{III}O\text{-}H]^{2+}$ can now be calculated. We have followed the protocol of Mayer in applying the Bordwell-Polanyi equation,

$$D_{O-H}=23.06\,E^{o}+1.37\,pK_a+C \quad (1)$$

to C-H bond oxidations by a number of metal-oxo complexes.[30] However, eqn 1 applies only to a system where the E^o value for the $(M_{ox}=O)/(M_{red}-O^-)$ couple and the pK_a value of the M_{red}–O-H species can be measured independently. In a process where electron transfer and proton transfer steps cannot be separated, such as the reduction of an Fe^{IV}=O species like **1** to an Fe^{III}-OH species, the $E_{1/2}(Fe^{IV/III})$ value already includes both e^- and H^+ affinity contributions. What remains to be included is the pH of the solution, which is correlated with the $E_{1/2}$ value by the Pourbaix plot. Therefore, a modified Bordwell-Polanyi equation,

$$D_{O-H}=23.06\,E_{1/2}(Fe^{IV/III})+1.37\,pH+C, \quad (2)$$

was used. For aqueous solutions with $E_{1/2}$ vs. SCE, C = 63 ± 2 kcal mol^{-1}.[31] Using eqn 2, we calculate D_{O-H} for $[Fe^{III}(N4Py)O-H]^{2+}$ to be 78(2) kcal mol^{-1}. Based on available data in the literature, the D_{O-H} associated with **1** is at the low end of the range of values listed in Table 1 that are associated with several Mn-oxo species (75–84 kcal mol^{-1}),[30,32-34] $[Ru^{IV}(O)(bpy)_2(py)]^{2+}$ (84 kcal mol^{-1}),[35] and $[Fe^{IV}(O)(TSMP)]$ (90 kcal mol^{-1})[28,29] Thus **1** would appear to have a much lower thermodynamic driving force for H-atom abstraction than many of the complexes in Table 1.

This difference has led us to compare C-H bond cleavage rates of the nonheme Fe^{IV}=O complex **1** with other metal-oxo complexes including heme Fe^{IV}=O, Ru^{IV}=O and several Mn-oxo complexes. Figure 7 shows a plot of the logarithm of the second order rate constant (log k_2) for dihydroanthracene (DHA) oxidation at 25 °C by various metal-oxo species vs. the D_{O-H} values associated with the oxidants. The straight line in the plot is defined by the appropriate values for ^{t}BuO• and ^{t}BuOO•, following Mayer's precedent.[35] We determined the rate of DHA oxidation by **1** in CH_3CN at 25 °C to be 18(1) $M^{-1}s^{-1}$ and compared this value to those of a variety of Mn-oxo complexes.[32-34,36] Interestingly, the points for the Mn complexes either fall onto the line or below it, while the point corresponding to **1** falls well above this line. Indeed, as shown in Table 1, the Mn complexes react with DHA by a factor of 10^2 – 10^5 more slowly than **1**, even though several of the Mn complexes have larger D_{O-H} values than **1**.

The apparently higher than expected relative reactivity of **1** still holds true when extended to ^{t}BuOO•, $[Fe^{IV}(O)(TMP)]$ (TMP = tetramesitylporphinate), and $[Ru^{IV}(O)(bpy)_2(py)]^{2+}$. We note that the DHA oxidation rate of **1** is comparable with the one reported for ^{t}BuOO•, despite the fact that its D_{O-H} of 89 kcal mol^{-1} is 11 kcal mol^{-1} higher than for **1**. Along a similar vein,, the k_2 for DHA oxidation by $[Fe^{IV}(O)(TMP)]$ at -15 °C measured by van Eldik is 2.7(1) $M^{-1}s^{-1}$,[37] essentially identical to the value of 2.8(1) $M^{-1}s^{-1}$ we have determined for **1** at -15 ° C. Unfortunately, the redox properties of $[Fe^{IV}(O)(TMP)]$ in aqueous solution cannot be established because of its insolubility in H_2O. However, as mentioned earlier, the redox potential of the related $[Fe^{IV}(O)(TSMP)]$ complex has been determined by cyclic voltammetry in aqueous solution, and a D_{O-H} value of 90 kcal mol^{-1} can be calculated from eqn 2 based on this work. From a systematic study of substituent effects on the redox potential of the Fe^{IV}=O/Fe^{III}-OH couple in CH_2Cl_2 by Groves,[38] we can then estimate that the loss of the sulfonate substituents should result in a decrease of about 0.1 V in the $Fe^{IV/III}$ potential for $[Fe^{IV}(O)(TMP)]$ and a corresponding decrease in its D_{O-H} value to 88 kcal mol^{-1}. Thus, despite the large difference in the thermodynamic driving force of 10 kcal mol^{-1}, **1** and $[Fe^{IV}(O)(TMP)]$ are comparable in their ability to oxidize DHA at -15 °C. Lastly, Mayer reported that $[Ru^{IV}(O)(bpy)_2(py)]^{2+}$ (D_{O-H} = 84 kcal mol^{-1}) oxidizes DHA at 25 °C in CH_3CN with a k_2 of

1.25×10^2 $M^{-1}s^{-1}$.[35] This value is a factor of 7 larger than the corresponding k_2 for **1** of 18 $M^{-1}s^{-1}$ or about a 1-kcal mol^{-1} difference in activation barrier; yet $[Ru^{IV}(O)(bpy)_2(py)]^{2+}$ has a D_{O-H} value that is 6 kcal mol^{-1} higher than for **1**. Taken together, our comparisons suggest that the C-H bond oxidizing power of **1** is higher than is reflected by its relatively small D_{O-H} value.

The data summarized in Figure 7 and Table 1 clearly cannot be rationalized by invoking thermodynamic arguments alone, and kinetic considerations must presumably be factored in. On the basis of DFT calculations, Shaik and co-workers have proposed the notion of two-state reactivity (TSR) to explain the behavior of **1**.[39,40] According to the TSR model, **1** has an S = 1 ground state, as established experimentally, and a nearby S = 2 excited state. The activation barrier for C-H bond cleavage is higher for the S = 1 ground state than for the S = 2 excited state, and spin crossover occurs as the reaction progresses along the reaction coordinate such that the rate-determining hydrogen atom abstraction by **1** occurs on the lower-lying quintet state surface. We postulate that this unique situation confers a kinetic advantage on **1** that compensates for its deficiency of thermodynamic driving force and enhances the C-H bond cleavage ability of the Fe^{IV}=O unit.

4. Concluding Remarks

Our work represents the first comprehensive electrochemical study on the redox properties of a nonheme Fe^{IV}=O complex in nonaqueous and aqueous solutions. In aqueous solution, reversible CV waves have been observed for the first time for the $Fe^{IV/III}$ couple of **1**. The transfer of one proton associated with the 1-e^- process that converts the Fe^{IV}=O unit to an Fe^{III}-OH species has been demonstrated by the Pourbaix plot (Figure 5). The CV behavior of **1** in CH_3CN has shown more complexity, which is likely associated with at least one additional chemical equilibrium and redox couple, as proposed in Scheme 1. C-H bond oxidations by **1** have been investigated also in aqueous solution and the reaction rates exhibit no solvent dependence. The $D(Fe^{III}O-H)$ of 78 kcal mol^{-1} calculated from the electrochemistry data of **1** falls at the low end of the range of values associated with other metal-oxo complexes. This value is also lower than values (84 and 97 kcal mol^{-1}) predicted by recent DFT calculations of **1**.[39-41] However, the reaction rate of **1** with DHA is comparable to those of oxidants having D_{O-H} values that are 6-11 kcal mol^{-1} higher (Figure 7, Table 1), implying the existence of a kinetic advantage for **1** that can compensate for its lower thermodynamic driving force. When extended to oxygen activating iron enzymes, these results suggest that the ligand environments of the nonheme subset may be particularly tuned to enable their Fe^{IV}=O units to carry out H-atom abstractions efficiently. Future efforts are aimed at extending the electrochemistry studies in aqueous solution to other Fe^{IV}=O complexes.

Supplementary Material

Refer to Web version on PubMed Central for supplementary material.

Acknowledgments

We gratefully acknowledge NIH grant GM-33162 (L.Q.) for support of this work and Profs. M. J. Collins and C. Kubiak for valuable discussions.

References

1. Riggs-Gelasco PJ, Price JC, Guyer RB, Brehm JH, Barr EW, Bollinger JM Jr, Krebs C. J Am Chem Soc 2004;126:8108–8109. [PubMed: 15225039]
2. Hoffart LM, Barr EW, Guyer RB, Bollinger JM Jr, Krebs C. Proc Natl Acad Sci USA 2006;103:14738–14743. [PubMed: 17003127]

3. Krebs C, Galonić Fujimori D, Walsh CT, Bollinger JM Jr. Acc Chem Res 2007;40:484–492. [PubMed: 17542550]
4. Galonic Fujimori D, Barr EW, Matthews ML, Koch GM, Yonce JR, Walsh CT, Bollinger JM Jr, Krebs C, Riggs-Gelasco PJ. J Am Chem Soc 2007;129:13408–13409. [PubMed: 17939667]
5. Shan X, Que L Jr. J Inorg Biochem 2006;100:421–433. [PubMed: 16530841]
6. Que L Jr. Acc Chem Res 2007;40:493–500. [PubMed: 17595051]
7. England J, Martinho M, Farquhar ER, Frisch JR, Bominaar EL, Münck E, Que L Jr. Angew Chem Int Ed 2009;48:3622–3626.
8. Rohde JU, In JH, Lim MH, Brennessel WW, Bukowski MR, Stubna A, Münck E, Nam W, Que L Jr. Science 2003;299:1037–1039. [PubMed: 12586936]
9. Klinker EJ, Kaizer J, Brennessel WW, Woodrum NL, Cramer CJ, Que L Jr. Angew Chem Int Ed 2005;44:3690–3694.
10. Thibon A, England J, Martinho M, Young VG Jr, Frisch JR, Guillot R, Girerd JJ, Münck E, Que L Jr, Banse F. Angew Chem Int Ed 2008;47:7064–7067.
11. Kaizer J, Klinker EJ, Oh NY, Rohde JU, Song WJ, Stubna A, Kim J, Münck E, Nam W, Que L Jr. J Am Chem Soc 2004;126:472–473. [PubMed: 14719937]
12. Klinker EJ, Shaik S, Hirao H, Que L Jr. Angew Chem Int Ed 2009;48:1291–1295.
13. Sastri CV, Oh K, Lee YJ, Seo MS, Shin W, Nam W. Angew Chem Int Ed 2006;45:3992–3995.
14. Collins MJ, Ray K, Que L. Inorg Chem 2006;45:8009–8011. [PubMed: 16999397]
15. Lee YM, Kotani H, Suenobu T, Nam W, Fukuzumi S. J Am Chem Soc 2008;130:434–435. [PubMed: 18085783]
16. Roelfes G, Lubben M, Chen K, Ho RYN, Meetsma A, Genseberger S, Hermant RM, Hage R, Mandal SK, Young VG Jr, Zang Y, Kooijman H, Spek AL, Que L Jr, Feringa BL. Inorg Chem 1999;38:1929–1936. [PubMed: 11670967]
17. Roelfes G, Vrajmasu V, Chen K, Ho RYN, Rohde JU, Zondervan C, la Crois RM, Schudde EP, Lutz M, Spek AL, Hage R, Feringa BL, Münck E, Que L Jr. Inorg Chem 2003;42:2639–2653. [PubMed: 12691572]
18. Laviron E. J Electroanal Chem 1984;164:213–227.
19. Sawyer, DT.; Sobkowiak, A.; Roberts, JL, Jr. Electrochemistry for chemists. Sawyer, DT.; Sobkowiak, A.; Roberts, JL., Jr, editors. John Wiley & Sons, Inc.; New York: 1995. p. 358-403.
20. Marmion ME, Takeuchi KJ. J Am Chem Soc 1988;110:1472–1480.
21. Moyer BA, Meyer TJ. Inorg Chem 1981;20:436–444.
22. Takeuchi KJ, Thompson MS, Pipes DW, Meyer TJ. Inorg Chem 1984;23:1845–1851.
23. Dovletoglou A, Adeyemi SA, Meyer TJ. Inorg Chem 1996;35:4120–4127. [PubMed: 11666620]
24. Hirai Y, Kojima T, Mizutani Y, Shiota Y, Yoshizawa K, Fukuzumi S. Angew Chem Int Ed 2008;47:5772–5776.
25. Lubben M, Meetsma A, Wilkinson EC, Feringa B, Que L Jr. Angew Chem Int Ed Engl 1995;34:1512–1514.
26. Fukuzumi S, Kotani H, Suenobu T, Hong S, Lee YM, Nam W. Chem Eur J 2010;16:354–361.
27. The simulation of the overall mechanism as formally a ET-PT process does not imply that the Fe^{III}-O^{-} species is an intermediate on the electrode surface. Pourbaix plots and simulations cannot distinguish between concerted proton coupled electron transfer (PCET) and stepwise ET-PT or PT-ET processes
28. Liu, Mh; Su, YO. J Electroanal Chem 1998;452:113–125.
29. Wolak M, van Eldik R. Chem Eur J 2007;13:4873–4883.
30. Mayer JM. Acc Chem Res 1998;31:441–450.
31. The value of C is 57 ± 2 kcal mol^{-1} in aqueous solution vs. NHE from ref 30. The potential of SCE is 0.2412 V vs. NHE. Therefore, the C value vs. SCE in aqueous solution (in kcal mol^{-1}) should be $57 + 0.2412 \times 23.06 = 62.6 \approx 63 \pm 2$
32. Wang K, Mayer JM. J Am Chem Soc 1997;119:1470–1471.
33. Yin G, Danby AM, Kitko D, Carter JD, Scheper WM, Busch DH. J Am Chem Soc 2007;129:1512–1513. [PubMed: 17249671]

34. Yin G, Danby AM, Kitko D, Carter JD, Scheper WM, Busch DH. J Am Chem Soc 2008;130:16245–16253. [PubMed: 18998682]
35. Bryant JR, Mayer JM. J Am Chem Soc 2003;125:10351–10361. [PubMed: 12926960]
36. Gardner KA, Kuehnert LL, Mayer JM. Inorg Chem 1997;36:2069–2078. [PubMed: 11669825]
37. Fertinger C, Hessenauer-Ilicheva N, Franke A, van Eldik R. Chem Eur J 2009;15:13435–13440.
38. Groves JT, Gross Z, Stern MK. Inorg Chem 1994;33:5065–5072.
39. Kumar D, Hirao H, Que L Jr, Shaik S. J Am Chem Soc 2005;127:8026–8027. [PubMed: 15926822]
40. Hirao H, Kumar D, Que L Jr, Shaik S. J Am Chem Soc 2006;128:8590–8606. [PubMed: 16802826]
41. de Visser SP. J Am Chem Soc 2010;132:1087–1097. [PubMed: 20041691]

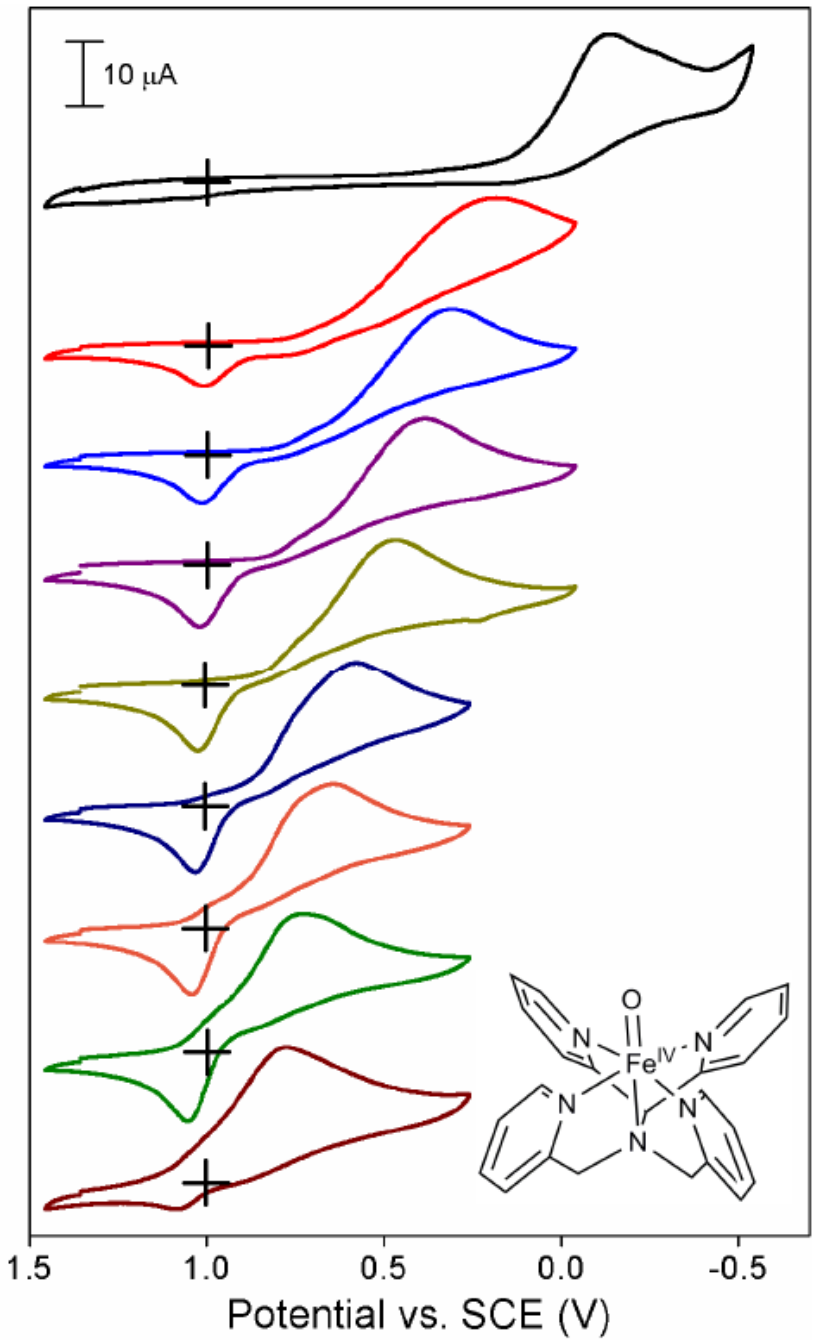

Figure 1.

CVs of **1** (structure shown) in dry CH_3CN at room temperature and a scan rate of 0.10 V s^{-1} with added CF_3COOH concentration of 0 M (black), 0.003 M (red), 0.01 M (blue), 0.03 M (purple), 0.1 M (dark yellow), 0.3 M (navy), 1 M (orange), 2 M (olive) and 5 M (wine). $E_{p,c}$ values are listed in Table S1. The crossing points indicate for each CV trace the coordinates where I = 0 μA and E = +1.0 V.

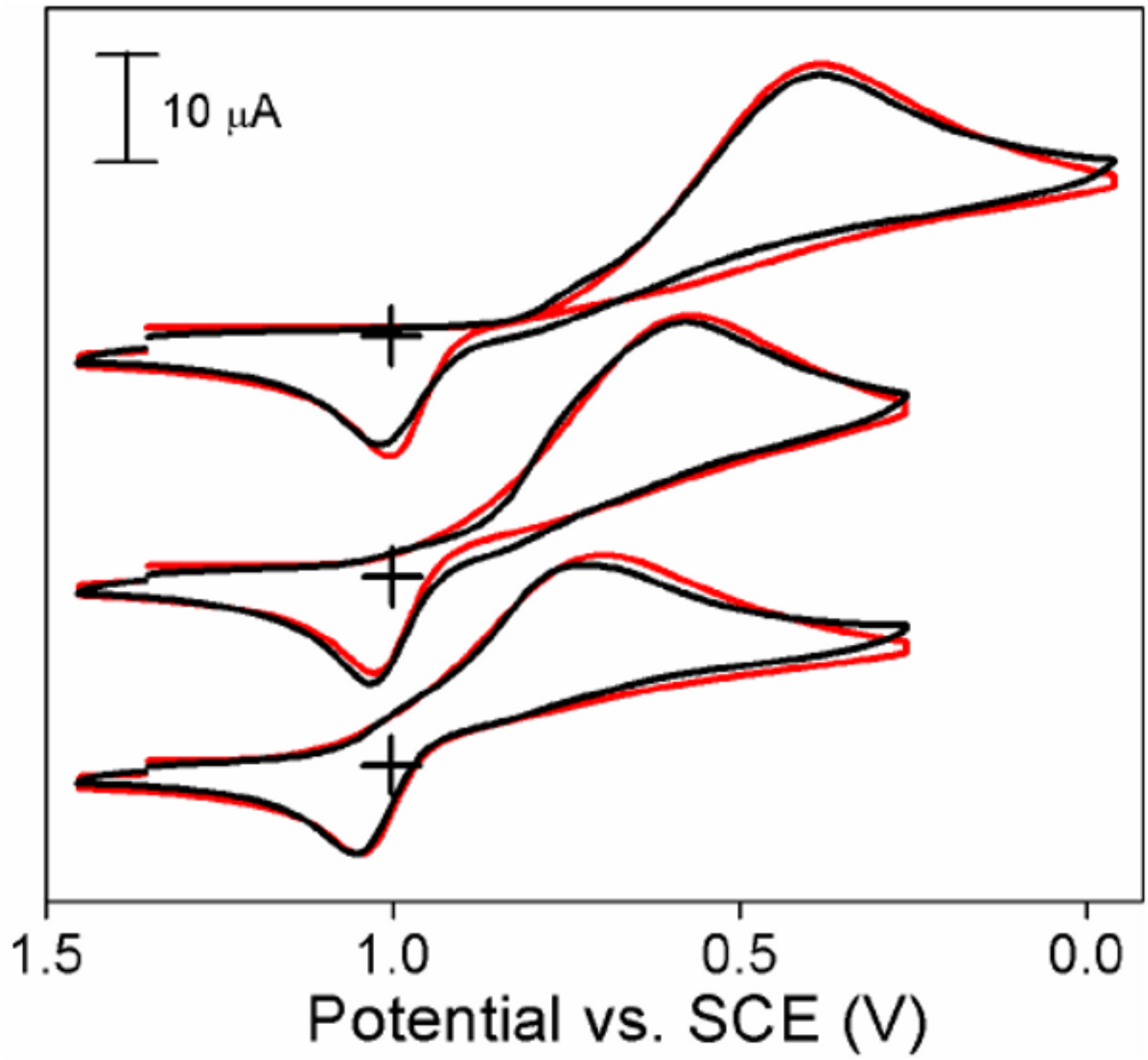

Figure 2.
Experimental (black lines) and fitted (red lines, according to Scheme 1) CVs of **1** in dry CH_3CN at room temperature and a scan rate of 0.10 V s^{-1} with added CF_3COOH concentration of 0.03 M (top), 0.3 M (middle) and 2 M (bottom). Simulation parameters and values are listed in Supporting Information. The crossing points indicate for each CV trace the coordinates where I = 0 μA and E = +1.0 V.

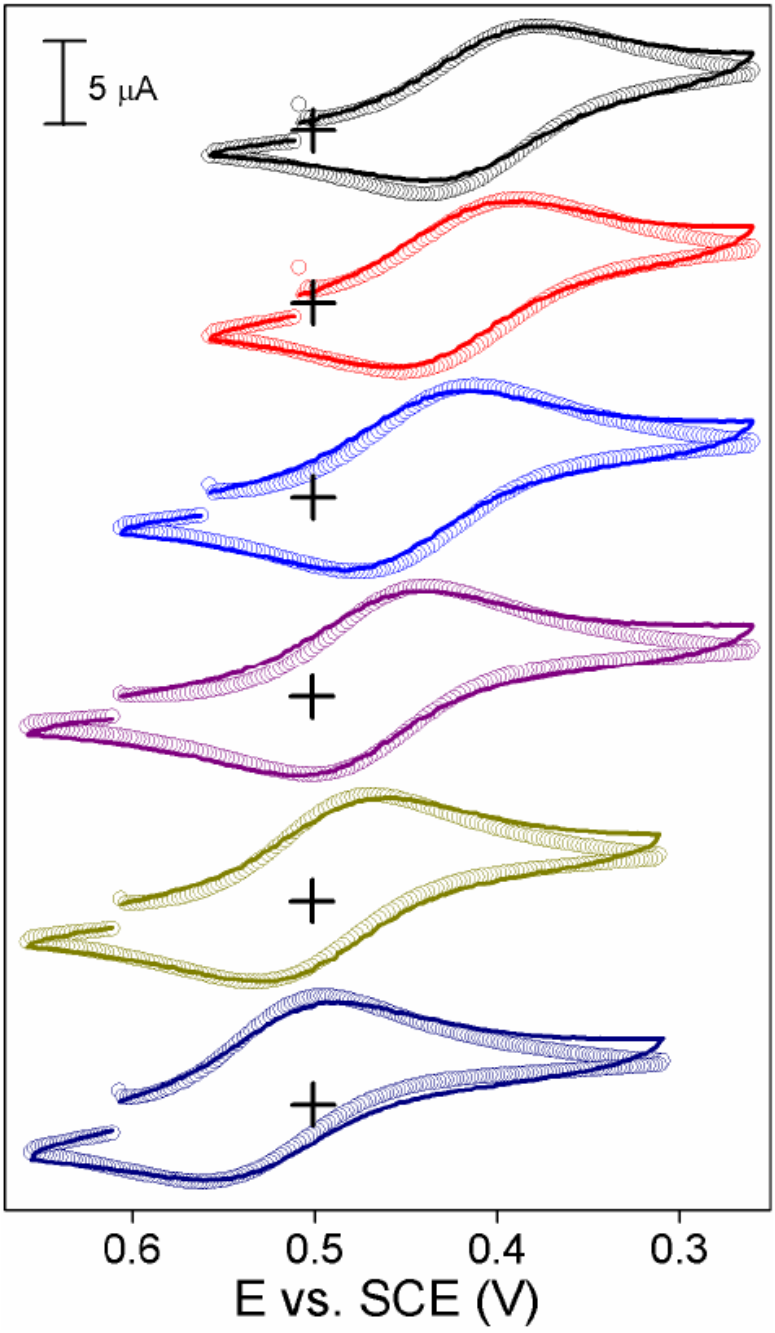

Figure 3.

Experimental (solid lines) and simulated (open circles, according to Scheme 2) CVs of **1** in H_2O at room temperature and a scan rate of 0.10 V s^{-1} at pH values of 4.01 (black), 3.51 (red), 2.92 (blue), 2.42 (purple), 2.02 (dark yellow) and 1.55 (navy). Simulation parameters and values are listed in Supporting Information. The crossing points indicate for each CV trace the coordinates where I = 0 μA and E = +0.5 V.

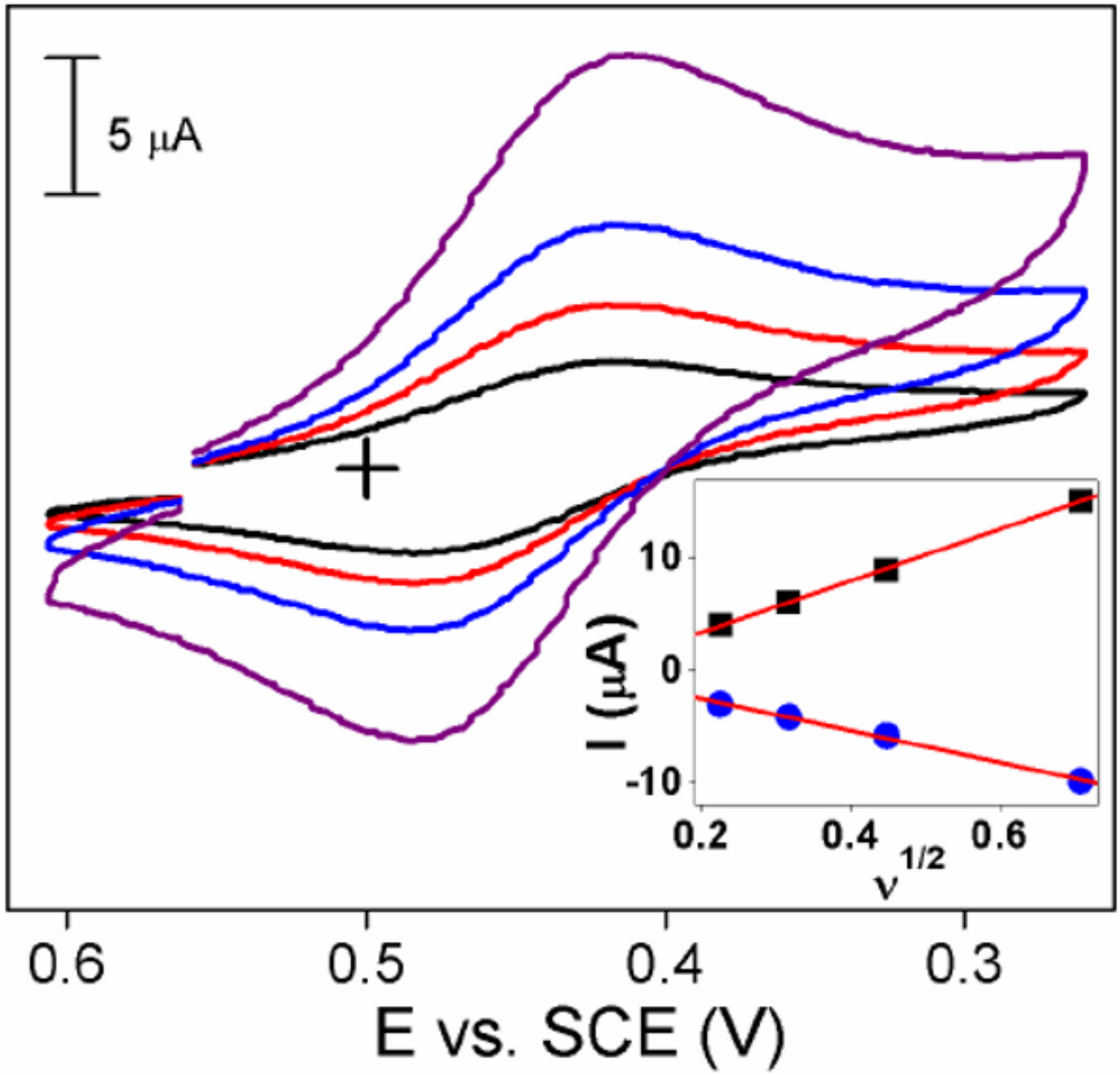

Figure 4.

CVs of **1** in H_2O at pH 2.92 at room temperature and scan rate of 0.05 V s^{-1} (black), 0.1 V s^{-1} (red), 0.2 V s^{-1} (blue), and 0.5 V s^{-1} (purple). Inset: plots of $I_{p,c}$ (black filled squares) and $I_{p,a}$ (blue filled circles) vs. the square root of the scan rate. The crossing point indicates the coordinates where I = 0 μA and E = +0.5 V.

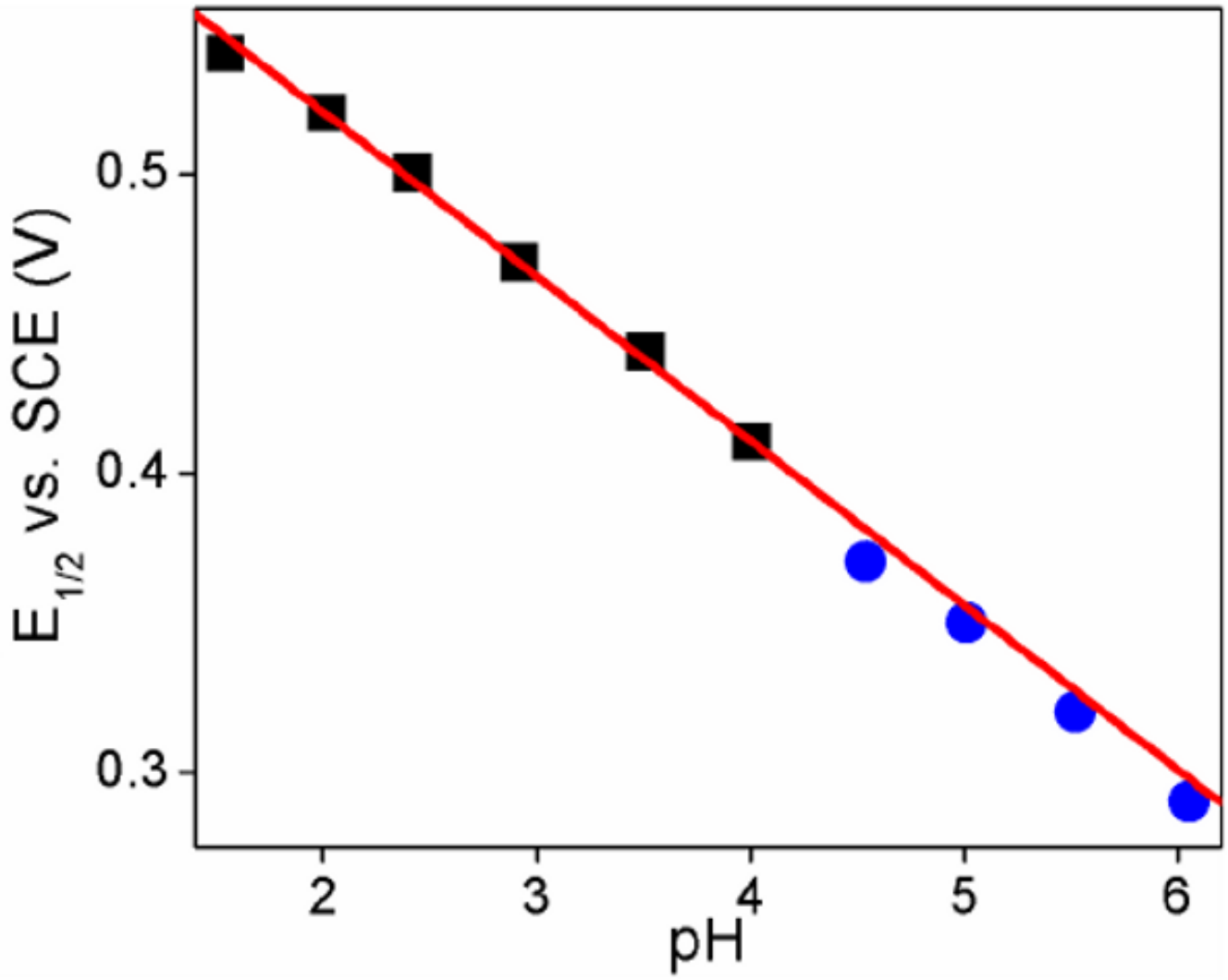

Figure 5.
Pourbaix plot of $E_{1/2}$ values vs. pH. $E_{1/2}$ values were obtained from reversible CVs at pH 1.5-4 (black filled squares) and CVs at pH 4-6, where the oxidative peak showed a reduced intensity (blue filled circles). The red line represents the linear fit of data points on the pH range of 1.5-4.

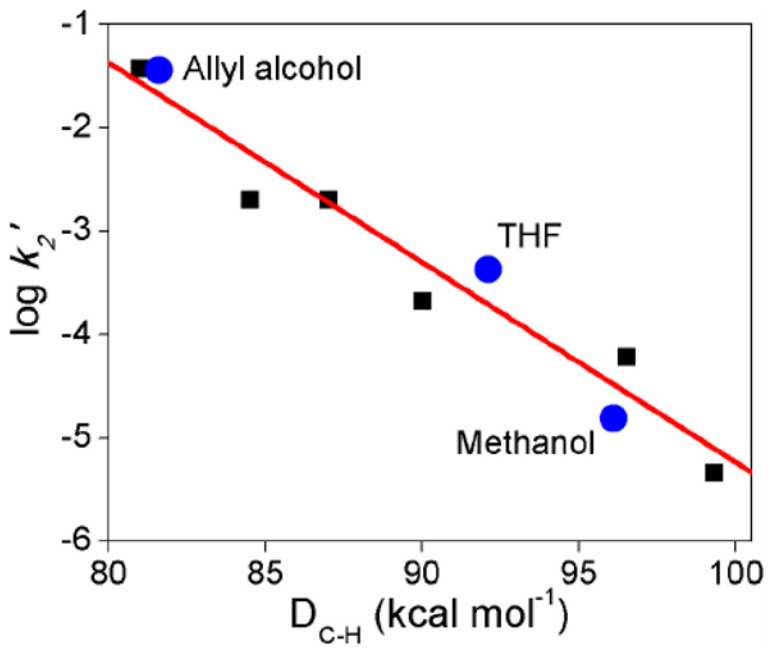

Figure 6.

Correlation (red line) of log k_2' and the C-H bond dissociation energies of hydrocarbons being cleaved in their reactions with **1** at 25 °C in CH_3CN[11,12] (black filled square) and H_2O (blue filled circle).

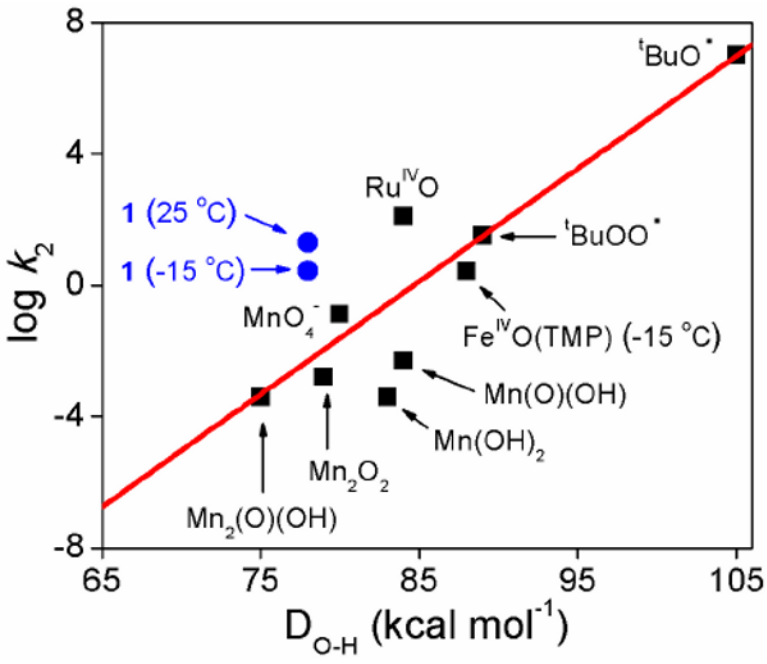

Figure 7.

Plot of log k_2 of DHA oxidation and the strength of O-H bond formed by the oxidants in CH_3CN at 25 °C unless labeled otherwise. Data points shown in black filled squares were taken from ref 32[-37]; and the blue filled circle obtained in the present work of complex **1**. The red straight line was drawn through the points belonging to the two oxygen radicals following Mayer's precedent. Mn(O)(OH): $[Mn^{IV}(Me_2EBC)(O)(OH)]^+$, $Mn(OH)_2$: $[Mn^{IV}(Me_2EBC)(OH)_2]^{2+}$, Mn_2O_2: $[(phen)_2Mn^{IV}(O)_2Mn^{III}(phen)_2]^{3+}$, Mn_2(O)(OH): $[(phen)_2Mn^{III}(O)(OH)Mn^{III}(phen)_2]^{3+}$, $Ru^{IV}O$: $[Ru^{IV}(O)(bpy)_2(py)]^{2+}$.

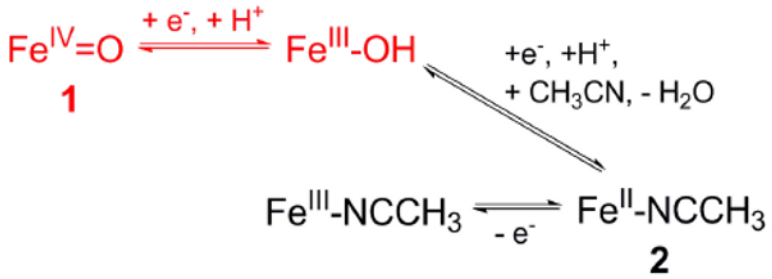

Scheme 1.
Proposed overall mechanism for the reduction of **1** in CH_3CN (the whole scheme) and H_2O (red portion).

Table 1

Redox potential, O-H bond strength of the 1-e$^-$ reduced form, and the second order rate constant for DHA oxidation of metal-oxo oxidants compared in Figure 7.

Complex	$E_{1/2}$ (pH) in H_2O vs. SCE (V)	D_{O-H} (kcal mol^{-1})	k_2[a] of DHA oxidation in CH_3CN (M^{-1} s^{-1})	Ref
1	0.24 (7) 0.18 (8)	78	18 2.8 (-15 °C)	This work
[Fe^{IV}(O)(TSMP)]	0.7 (8)	90	N.A.	28, 29
[Fe^{IV}(O)(TMP)]	N.A.	88[b]	2.7 (-15 °C)	37
$Ru^{IV}O$	0.53 (7)	84	1.25×10^2	35
MnO_4^-	0.32[c]	80	1.2×10^{-1}	36
[Mn^{IV} (Me_2EBC) (O) (OH)]$^+$	N.A.	84	5.6×10^{-3}	33,34
[Mn^{IV}(Me_2EBC)$(OH)_2$]$^{2+}$	N.A.	83	3.7×10^{-4}	33,34
[$(phen)_2Mn^{IV}(O)_2Mn^{III}(phen)_2$]$^{3+}$	N.A.	79	1.6×10^{-3}	32
[$(phen)2Mn^{III}(O)(OH)Mn^{III}(phen)_2$]$^{3+}$	N.A.	75	4.2×10^{-4}	32

[a] k_2 values were measured at 25 °C unless otherwise stated.

[b] This value was estimated, as mentioned in the text.

[c] This is the 1-e$^-$ potential of the MnO_4^-/ MnO_4^{2-} couple, which is not associated with H^+ transfer.